ASME Journal of Engineering for Gas Turbines and Power
Online journal at:
https://asmedigitalcollection.asme.org/gasturbinespower

High-Temperature Industrial-Scale CO_2 Heat Pumps: Thermodynamic Analysis and Pilot-Scale Testing

Timothy J. Held[1]
Echogen Power Systems,
365 Water Street,
Akron, OH 44308
e-mail: theld@echogen.com

Jason Miller
Echogen Power Systems,
365 Water Street,
Akron, OH 44308
e-mail: jmiller@echogen.com

Jason Mallinak
Echogen Power Systems,
365 Water Street,
Akron, OH 44308
e-mail: jmallinak@echogen.com

Luke Magyar
Echogen Power Systems,
365 Water Street,
Akron, OH 44308
e-mail: lmagyar@echogen.com

Electrification of heat-generating processes is a key means to decarbonize industrial emissions, and heat pumps significantly improve the efficiency of electrified heat. Carbon dioxide is one of the oldest known heat pump working fluids, but its use is presently limited to low-temperature (<120 °C) applications and, when operating in a transcritical mode, for heating liquid water and similar single-phase materials. Conventional subcritical hydrofluorocarbon (HFC) or hydrofluoroolefin (HFO) refrigerants also have temperature limitations due to thermal degradation and are subject to eventual phase-out. Finally, most smaller heat pump systems use oil-lubricated positive displacement compressors, which also impose temperature limitations due to the thermal stability of the entrained oil in the refrigerant. By taking advantage of oil-free, turbomachinery-based equipment and using CO_2 as the refrigerant, the temperature limitations of existing heat pump solutions can be eliminated. Novel cycle architectures, partially derived from sCO_2 power cycle concepts, have been developed that significantly improve the performance of CO_2 heat pumps relative to conventional vapor compression architectures, both for single-phase material heating and for medium pressure steam generation. Cycle simulations of these new heat pump cycles that cover a wide range of conditions and applications have been completed. Pilot-scale (<50 kW_{th}) demonstration systems have been built and tested, and their measured performance provides validating data for the simulated results. [DOI: 10.1115/1.4068029]

Keywords: supercritical carbon dioxide, heat pump

1 Introduction

In many industrial processes, heat is applied to one or more materials at a relatively high temperature. The most common method of creating this heat today is through the combustion of fossil fuels. However, as the world moves toward a carbon-free energy system, alternative means to provide industrial heat will be required [1,2]. While direct electrical heating with devices such as resistance, arc, or induction heaters can attain the necessary temperatures, the coefficient of performance (COP, defined as the amount of heat transferred to the process divided by the electrical power input) of these processes can never be greater than 1.0.

In contrast, thermodynamic heat pump cycles can attain COP values well in excess of 1.0. However, cycle and working fluid issues limit attainable heating temperatures in heat pumps today to less than 120 °C, with advanced technologies in development for up to 160 °C [3]. For instance, traditional hydrofluorocarbon (HFC) and hydrofluoroolefin (HFO) refrigerants thermally decompose at high temperatures (e.g., Refs. [4] and [5]), making them unsuitable for higher-temperature heat pump applications. In addition, upcoming regulations in some markets are likely to result in the phase-out of these types of refrigerants [6]. And finally, while some hydrocarbon refrigerants such as R600a (isobutane) and R601a (isopentane) are available for higher-temperature applications, their high flammability hazards represent a substantial risk for deployment in many applications.

A transcritical CO_2 heat pump can provide higher temperature than other refrigerants due to its thermal stability and supercritical state during the transfer of heat from the compressed CO_2 to the heat sink material. In particular, larger scale heat pumps (approximately 5 MW_{th} and larger class for CO_2) can use oil-free centrifugal compression to avoid thermal decomposition of the entrained lubricants that typically are used with smaller scale positive displacement compressors [7]. CO_2 has no flammability hazards, zero ozone depletion potential, and is a low global warming potential gas.

The thermophysical properties of CO_2 have a profound impact on the heat transfer processes both within and external to the heat pump cycle. Optimal performance of a CO_2 heat pump requires careful matching of the heat capacity characteristics of the working fluid and the heat source/sink fluids and innovative cycle designs. In this paper, we describe CO_2 heat pump cycles that serve two important but very different applications. Many applications involve heating a constant heat capacity fluid such as air or other single-phase material from a low to a high temperature. The second widely used process

[1]Corresponding author.

Manuscript received September 27, 2024; final manuscript received January 17, 2025; published online March 21, 2025. Editor: Jerzy T. Sawicki.

heating application is steam generation, which occurs at constant temperature. In these two applications, the heat transfer between the working and process fluids is fundamentally different and implies that different heat pump cycles will be required to optimize performance.

For lower-temperature applications, a conventional vapor compression heat pump cycle provides a good combination of performance and simplicity. Most commercial heat pumps today use HFC or HFO working fluids in a completely subcritical operating state. During the process of transferring heat to the sink, the working fluid condenses at constant temperature. This type of heat pump/working fluid combination can supply heat at temperatures up to approximately 150 °C [8], limited by working fluid and lubricant thermal stability. The working fluids that are usable at higher temperatures typically have low vapor pressures, which require vacuum evaporation and risk air ingestion when ambient temperature heat sources are used.

CO_2 heat pumps, especially for higher-temperature applications, typically operate in transcritical mode, where the fluid is supercritical from the compressor exit to the expander inlet, and subcritical over the remainder of the cycle. The high vapor pressure of CO_2 allows for efficient extraction of heat from low-temperature sources during its evaporation process, including ambient air or water. During the supercritical pressure process of transferring heat to the heat sink, the working fluid temperature continuously decreases. This makes CO_2 transcritical cycles ideal candidates for applications where the heat sink temperature needs to be increased over a wide $T_{\text{range}} (\equiv T_{s,h} - T_{s,c})$, such as domestic hot water heating, and where high-temperature waste heat sources are not available.

By using a transcritical CO_2 heat pump, limitations regarding working fluid stability are avoided, and a turbomachinery-based system can be designed without lubricant entrainment in the working fluid. However, practical considerations regarding pressure ratio and temperature glide-matching (defined and discussed in Sec. 2) in the high-temperature heat exchanger (HTX) impact the attainable performance of a conventional transcritical CO_2 heat pump for high temperature range and temperature lift. For instance, the required compressor pressure ratio of a simple nonrecuperated transcritical CO_2 heat pump to achieve 300 °C heat sink temperature is greater than 25:1 (Fig. 1), which would exceed typical industrial compressor discharge pressures.

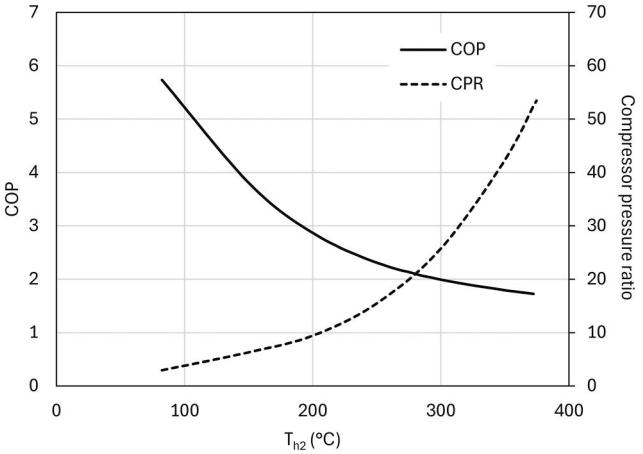

Fig. 1 Coefficient of performance and required compressor pressure ratio for the simple nonrecuperated cycle as a function of the maximum temperature of the heat sink ($T_{s,h}$). For these calculations, the initial temperature of the heat sink ($T_{s,c}$) is fixed at 20 °C, and the heat source is 15 °C.

2 High-Temperature CO_2 Heat Pumps

In this paper, we are focused on applications at higher temperatures than conventional heat pumps can supply, from 150 to 400 °C. These higher-temperature applications fall into two main categories:

(1) Large T_{range}: In these cases, the heat sink temperature needs to be raised from a relatively low to a high value, and the specific heat capacity ($c_p = \partial h/\partial T|_p$) is essentially constant. Examples include air heating for drying applications or process fluid heating.
(2) Zero T_{range}: When the heat sink undergoes a phase change, the heat sink temperature is constant during the phase transition process. The most common application is steam production.

2.1 High-Temperature Process Fluid Heating. To reduce the compressor pressure ratio required to achieve high heat sink temperatures, a recuperator (RCX) can be used to recover some of the residual enthalpy exiting the primary heat exchanger to preheat the fluid prior to entering the compressor. While the simple recuperated system can achieve high lift, it is limited by the recuperation process itself to relatively high working fluid temperature exiting the HTX. The reason for this is that the temperature–heat transferred (TQ) curves of the fluids in the HTX have markedly different slopes (sometimes called temperature glide, or $dT/dQ = (\dot{m}c_p)^{-1}$), which represent exergy loss in the HTX [9]. In addition, the large mismatch of specific heat capacity values at the different pressures within the system also results in a major slope difference in the recuperator TQ plot, further adding exergy destruction to the cycle and reducing its performance (Fig. 2).

To address these limitations, Echogen has developed a new high-temperature heat pump (HTHP) cycle [10] (Fig. 3) based on the

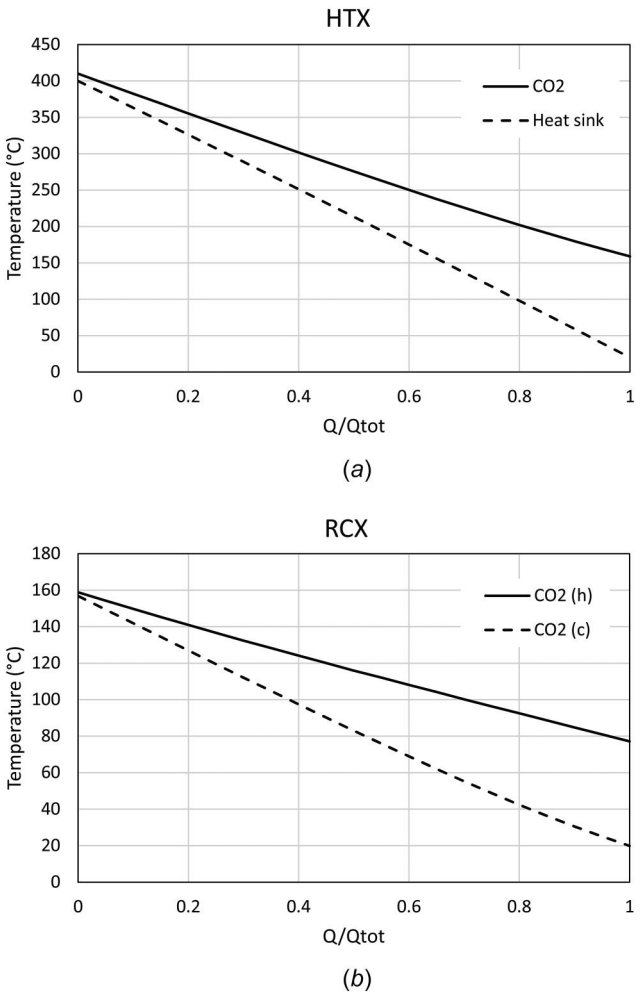

Fig. 2 TQ plots for the simple recuperated cycle, HTX and RCX

architecture of its waste heat recovery cycle [11], but operating in the reverse direction. In one version of this cycle, the HTX is divided into two stages. In the first stage, the working fluid transfers heat to the heat sink, heating the sink medium and cooling the working fluid. Upon exiting HTX1 (state 3), the working fluid is then divided into two portions. The first portion (state 3A) enters HTX2, where it is further cooled, and preheats the heat sink medium, which is counterflowing relative to the working fluid. The second portion (state 3B) enters an RCX, where it also is cooled and preheats the working fluid on the low-pressure side of the system (process 7 to 1). Upon exiting HTX2 (state 4A) and the recuperator (state 4B), the flows recombine (state 4). The flow then enters the expander (state 5) as in the simple recuperated cycle, where work is extracted, and the working fluid pressure and temperature are reduced (state 6). Heat is then added from a relatively low-temperature source (process 6 to 7), closing the cycle.

The division of the working fluid into two portions allows for better matching of the heat capacities ($C = \dot{m}c_p$) in the two sides of the recuperator (Fig. 4). In addition, the working fluid can be cooled to a lower temperature than it can in the single recuperated cycle, which also allows its TQ slope to better match the heat sink thermal slope (Fig. 4). Both effects reduce the exergy destruction of the cycle and improve its performance.

To better understand the implication of the refrigerant state during the heat transfer process to the heat sink, we can consider the fundamental performance parameters associated with the classical heat pump cycle. The limiting performance for a theoretical heat pump transferring heat between two infinite, constant temperature thermal reservoirs is determined by the well-known Carnot equation

$$\mathrm{COP} = (1 - T_c/T_h)^{-1} \tag{1}$$

where T_c and T_h are the temperatures of the infinite cold and hot reservoirs (heat source and sink), respectively. However, in the case of a finite reservoir, the reservoir temperature will vary as heat is extracted or added. By integrating over a range of infinitesimal reservoirs between the initial and final temperatures of the reservoir, one can derive that for a constant c_p reservoir material, Eq. (1) still applies with the reservoir temperatures replaced by the thermodynamic (or Lorenz) mean temperatures [12]

$$\bar{T} = \frac{T_{\max} - T_{\min}}{\ln(T_{\max}/T_{\min})} \tag{2}$$

where $T_{\max}$ and $T_{\min}$ represent the temperatures of the reservoirs at the beginning and end of the heat transfer process. Interestingly, the Lorenz COP exceeds the Carnot COP for finite reservoirs, leading to the somewhat counterintuitive result that for a fixed $T_{s,h,max}$, the ideal COP increases as the heat sink temperature range ($T_{s,h,\max} - T_{s,h,\min}$) increases.

In the idealized Carnot and Lorenz cycle cases, heat transfer between the thermal reservoirs and the refrigerant fluid is considered to be perfect, with no temperature difference between the two. We can consider the impact of finite-rate heat transfer by incorporating a simplified heat exchanger model into the analysis. The Lorenz COP is calculated on the basis of the refrigerant fluid temperatures, and the difference between the heat sink and fluid temperature is calculated by a simple heat exchanger conductance (UA) equation

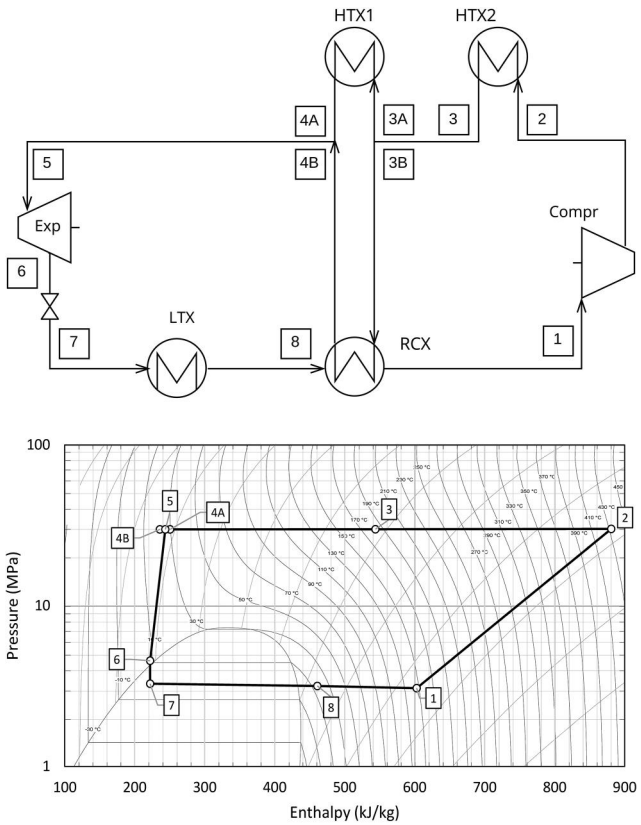

Fig. 3 Advanced recuperated cycle process flow and pressure–enthalpy diagrams

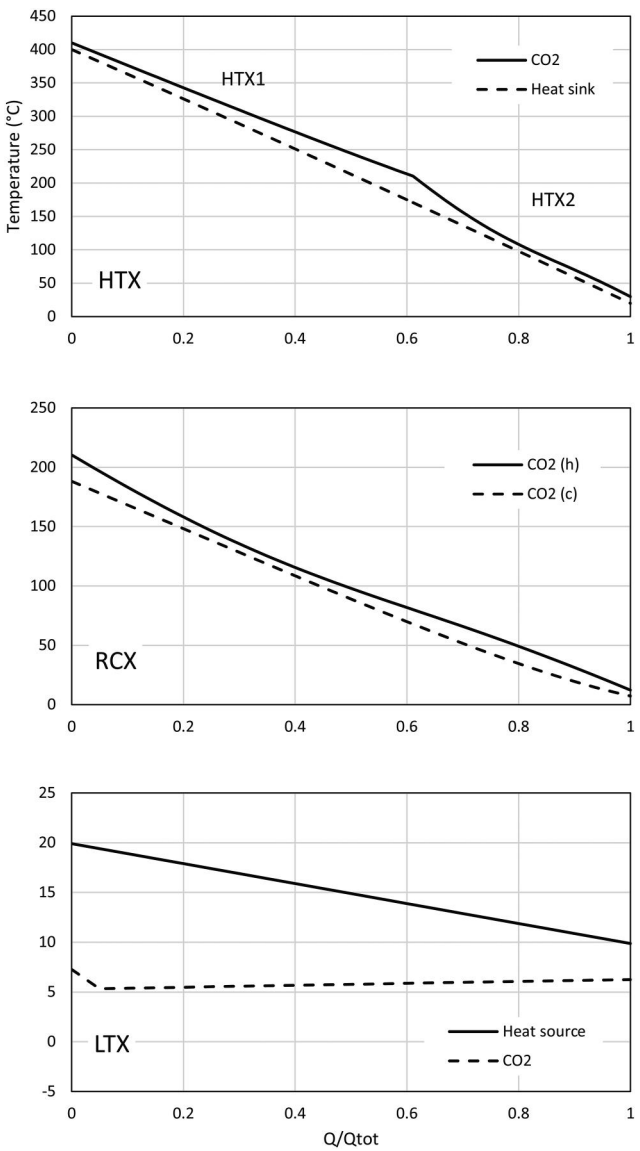

Fig. 4 TQ plots for heat exchangers in Fig. 3

$$Q = \mathrm{UA}\,\Delta T_{\mathrm{LM}} \tag{3}$$

We consider two limiting cases. For a subcritical heat pump, the fluid temperature is constant through the heat transfer process, resulting in the expression

$$\Delta T_{\mathrm{LM,sub}} = \frac{T_{s,h} - T_{s,c}}{\ln\left(\frac{T_f - T_{s,h}}{T_f - T_{s,h}}\right)} \tag{4}$$

For the transcritical case, we assume that the temperature difference between the heat sink and fluid is constant, and thus

$$\Delta T_{\mathrm{LM,sup}} = T_{f,\max} - T_{s,h} = T_{f,\min} - T_{s,c} \tag{5}$$

Using these two expressions to calculate the fluid temperatures required for the same heat sink temperature limits (Fig. 5), we can calculate the Lorenz COP for both the subcritical and transcritical cycles (Fig. 6). We can observe that as UA and $T_{s,h} - T_{s,c}$ increase, the advantage of the transcritical cycle over the subcritical cycle for this application increases. Only in the limit of small UA and heat sink temperature range does the subcritical cycle COP approach the transcritical cycle value, and indeed never exceeds it.

However, the specific heat capacity of CO_2 at the supercritical state and moderate temperature is a strong function of both temperature and pressure. Exergy analysis [9] shows that the most efficient heat transfer process in a counterflow heat exchanger is one in which the TQ curves of the two materials are parallel. The flexibility of the HTHP cycle allows the CO_2 TQ curve to be divided into multiple segments by varying the proportion of the CO_2 flowrate through each section of the HTX. As the slope is proportional to $1/(\dot{m}c_p)$, this variation in $\dot{m}_{CO_2}$ allows close matching of the TQ slopes of the two materials. This cycle innovation results in significant improvement in COP, as well as reduces the required compressor pressure ratio to achieve a target heat sink temperature.

The performance of the HTHP is calculated by system modeling as a function of the heat source temperature and heat sink peak temperature (Fig. 7). The system modeling approach follows the general practice as outlined in Refs. [11] and [13]. For the design basis calculations, fixed turbomachinery adiabatic isentropic efficiency values of 80% were used throughout, and fixed heat exchanger pressure drops of 0.1 MPa were assumed. For each set of boundary conditions ($T_{\mathrm{source,in}}$, $T_{s,h}$, and $T_{s,c}$), a constrained COP optimization exercise was conducted, with constraints including $\Delta T_{\min}$ for all heat exchangers, and the total UA for the summation of the HTX, LTX, and RCX heat exchangers as a simplified surrogate for system cost. Note that for all cases, the temperature reduction of the heat source was fixed at 10 K. In addition, a maximum

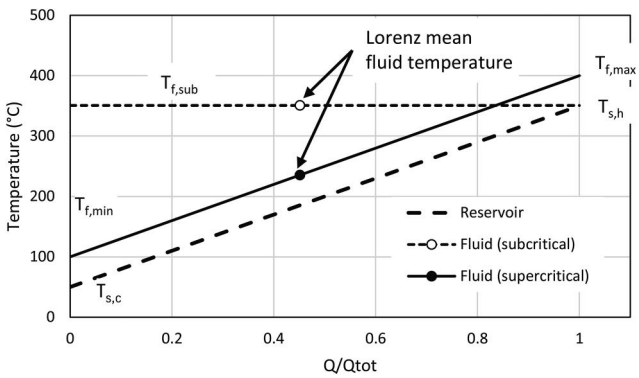

Fig. 5 Temperature–heat transfer plot for the high-temperature heat exchanger with $T_{s,h} = 350\,^{\circ}\mathrm{C}$, $T_{s,c} = 100\,^{\circ}\mathrm{C}$, and $Q/\mathrm{UA} = 50$ K. Fluid temperatures represent limiting subcritical (constant temperature condensation) and supercritical (constant specific heat capacity) cases.

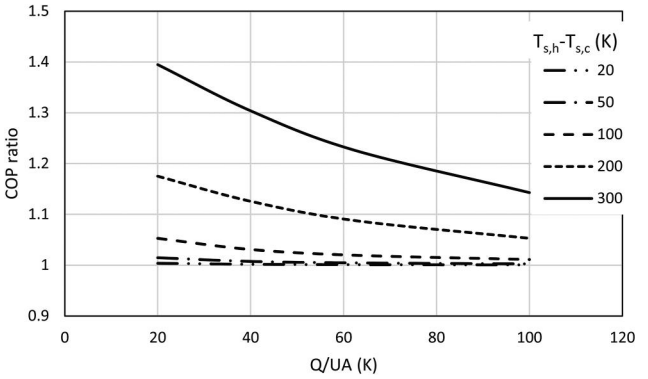

Fig. 6 Ratio of Lorenz ideal COP for transcritical and subcritical heat pump cycles for $T_{s,h} = 350\,^{\circ}\mathrm{C}$. The COP ratio asymptotically approaches unity as UA and $T_{s,h} - T_{s,c}$ each approach zero.

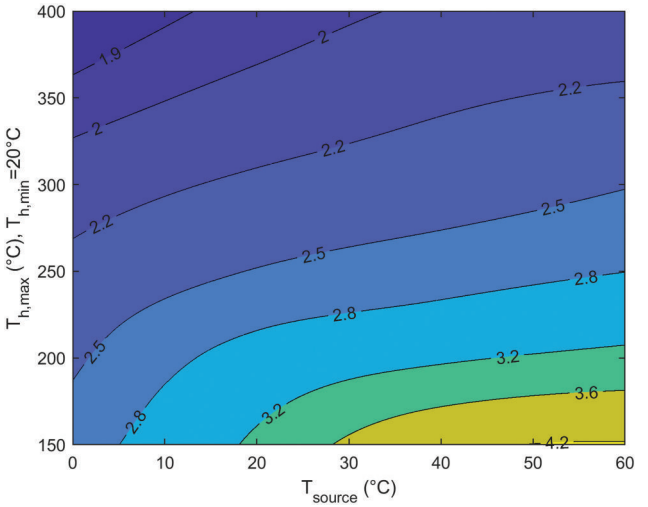

Fig. 7 COP map for CO_2 HTHP, when heating air from an initial temperature of 20 °C

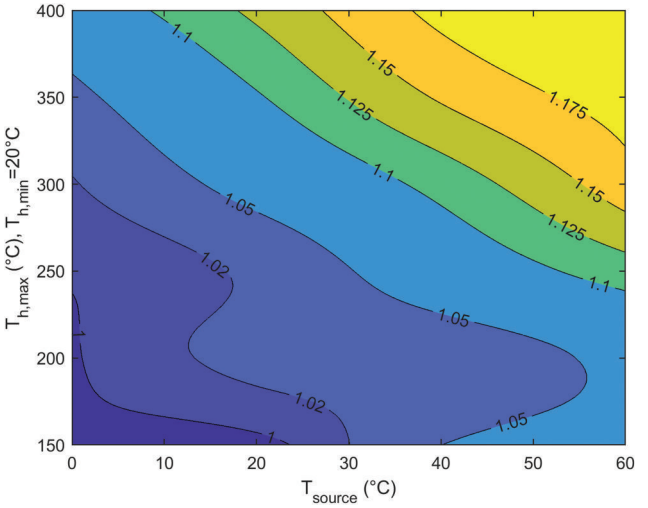

Fig. 8 Coefficient of performance ratio between simple recuperated heat pump and HTHP advanced cycle, when heating air from an initial temperature of 20 °C

compressor outlet pressure limit of 30 MPa was imposed to remain within typical piping component ranges. Optimization variables included compressor inlet and outlet pressures, and heat exchanger sizing.

The calculations were conducted over a range of heat source temperatures from 0 to 60 °C and $T_{s,h}$ from 150 to 400 °C (Fig. 7). A set of calculations were also performed for a simple recuperated cycle over the same range of conditions and the same constraints, with the COP ratio between the two cycles shown in Fig. 8. In general, the compressor pressure ratio and maximum compressor pressure were much lower with the HTHP cycle than the simple recuperated cycle.

2.2 Steam Generation. The process of steam generation has a fundamentally different character from the process fluid heating case above and requires a different approach to heat pump design. Steam generation is a phase-change process that occurs at constant temperature, and thus a transcritical heat pump is disadvantaged compared to a subcritical heat pump, in that the average temperature of heat transfer for the transcritical case will be significantly higher than for the subcritical case. While COP-based performance will be lower for a transcritical cycle, other advantages relative to the subcritical cycle are available. A fundamental challenge with direct steam generation from a subcritical heat pump is the available condensation temperature of the refrigerant, which must be significantly less (typically 20 to 30 K) than the fluid critical temperature. Typical HFC and HFO refrigerants have relatively low critical temperatures that therefore limit steam generation to low pressure (typically 2 barg or less) [14].

For applications requiring higher steam pressures, mechanical vapor compression of the low-pressure steam can be used to boost the delivered pressure, at the incremental cost and complexity of the additional mechanical equipment. High critical temperature refrigerants typically have high normal boiling points as well, requiring a cascade approach to avoid vacuum operation on the low-pressure side of the heat pump if ambient temperature heat sources are to be used. The limited selection of refrigerants that meet the combination of critical temperatures above 150 °C and normal boiling points below 15 °C include only R600 (normal butane) and HFOs R1224 yd(Z) and R1234ze(Z) [15].

Another key factor in achieving economic decarbonization of industrial heating systems is the use of energy storage to mitigate the variability in renewable electricity generation capacity and price. In comparisons of constant-rate electric heating plus electricity storage versus variable-rate electric heating integrated with thermal energy storage, the economic advantages of the latter approach were clear [16]. While the referenced study was performed for direct electric heating, the same factors would apply to heat pump applications. Subcritical heat pumps deliver heat at constant temperature, thus limiting the type of thermal storage that can be integrated to phase-change materials. Conversely, a transcritical heat pump delivers thermal energy over a finite range of temperatures, enabling thermal storage using low-cost, widely available sensible enthalpy storage materials such as two-tank fluid storage, packed-bed thermocline, and particulate material beds.

Direct steam generation from a transcritical cycle would require an extremely high compressor discharge pressure and temperature. As noted in Sec. 2.1, the addition of a recuperator to the simple cycle lowers the temperature range of the working fluid. However, for the steam generator application, this approach is of limited value. For instance, a simple recuperated heat pump, when generating 16.5 bar (a) steam ($T_{sat} = 203$ °C), is required to operate at a very high compressor discharge temperature to avoid a pinch restriction at the right-hand side of the TQ plot (Fig. 9).

Another potential issue with this configuration is the discharge state of the expander (state 5 in Fig. 10(*a*)), which can be seen on the corresponding pressure–enthalpy (PH) diagram to fall squarely within the vapor dome (Fig. 10(*b*)). Thus, a significant fraction of the expanded fluid will have flashed to the vapor state in the later stages of the expander, which could substantially affect both the performance and the durability of this device.

Finally, the COP of this cycle is limited as the Lorenz mean temperature of the high-temperature heat addition process is relatively high. For this example, $\bar{T}_{f,h} = 321$ °C, and the predicted COP is 1.48. To reduce $\bar{T}_{m,h}$, one can split the compression processes into two or more separate stages and extract heat between each. While this approach does reduce $\bar{T}_{f,h}$ to 261 °C, the COP only raises slightly to 1.50, and the expansion into the dome persists. The fundamental problem with this cycle (at least while using CO_2 as the working fluid) is that the large dependence of heat capacity on temperature and pressure causes a mismatch in the temperature "glide" between the low-pressure and high-pressure sides of the recuperator. This causes a large temperature difference between the high-pressure CO_2 exit and the low-pressure CO_2 entrance of the

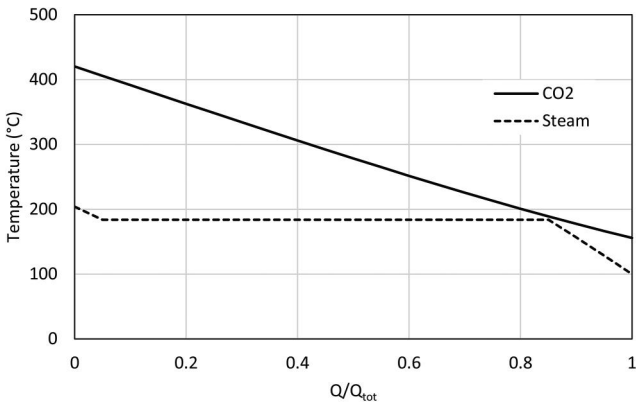

Fig. 9 Simple recuperated cycle steam generator temperature–heat transferred plot

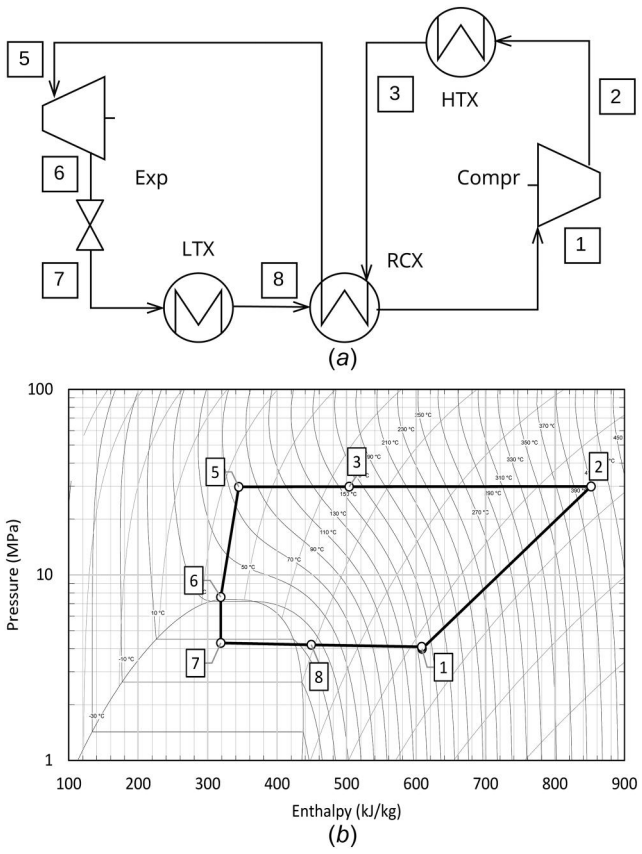

Fig. 10 Simple recuperated cycle process flow and pressure–enthalpy diagrams

recuperator, which in turn represents a large exergy destruction in the recuperator and thus a loss in performance.

The new heat pump steam generator (HPSG) cycle [17] (Fig. 11) addresses the heat capacity mismatch between the two fluid streams by dividing the flow at the outlet of steam generator 1 (SG1) and expanding a portion directly through a turbine (expander). The fraction of the total mass flowrate at state 60 is roughly proportional to the ratio of the specific heat capacities at states 60 and 70, such that $\dot{m}_{60}c_{p,60} = \dot{m}_{70}c_{p,70}$. This cycle increases the COP markedly over the previous two cycles. For this set of assumptions, the COP is 1.63, versus 1.50 for the previous best prediction. The improvement in performance is due to several factors:

(1) The mean temperature of the high-temperature fluid $\bar{T}_{f,h}$ is further reduced to 256 °C using the same steam conditions as the previous analysis.
(2) The heat capacity of the two flow streams in the recuperator is now well-matched, significantly reducing the exergy destruction in that heat exchanger.
(3) The work recovered in expander 1 offsets a portion of the compressor work.
(4) By better matching the heat capacities of the two streams, a much lower temperature at state 61 can be achieved. Thus, the lower-temperature expander (expander 2) exit is now a single-phase liquid or low-vapor level mixture of liquid and vapor. The higher-temperature expander (expander 1) exit is also single-phase, on the vapor side of the two-phase region.

Using the same modeling techniques and assumptions as described in Sec. 2.1, simulations over a range of heat source temperatures and steam saturation pressures have been conducted using the new HPSG configuration (Fig. 12).

For comparison, a model of a two-stage subcritical vapor compression heat pump was created using the same modeling approach as for the CO_2 HPSG, with R1233zd(E) as the refrigerant and a 40 °C heat source (lower heat source temperatures required subatmospheric low-side pressure, or a separate cascaded heat pump with a lower normal boiling point refrigerant). Atmospheric pressure steam was generated by the vapor compression heat pump and compressed to higher pressure in a two-stage steam compressor with boiler feedwater injection between stages. The COP calculated using this cycle was 2.24, or 12% higher than the HPSG at the same conditions. Although from a strict performance perspective, the HPSG cannot match the vapor compression plus steam compression system, the other advantages of the HPSG are significant:

- Operational simplicity: Steam can be generated directly in a single heat pump at pressures well above 20 barg.
- Low-temperature heat source capability: CO_2 heat pumps can effectively use heat from sources that are well below 0 °C due to the high vapor pressure of CO_2.
- Thermal storage integration: Due to the large temperature differential in the SG1 and SG2 heat exchangers, conventional sensible enthalpy thermal energy storage materials can be used.

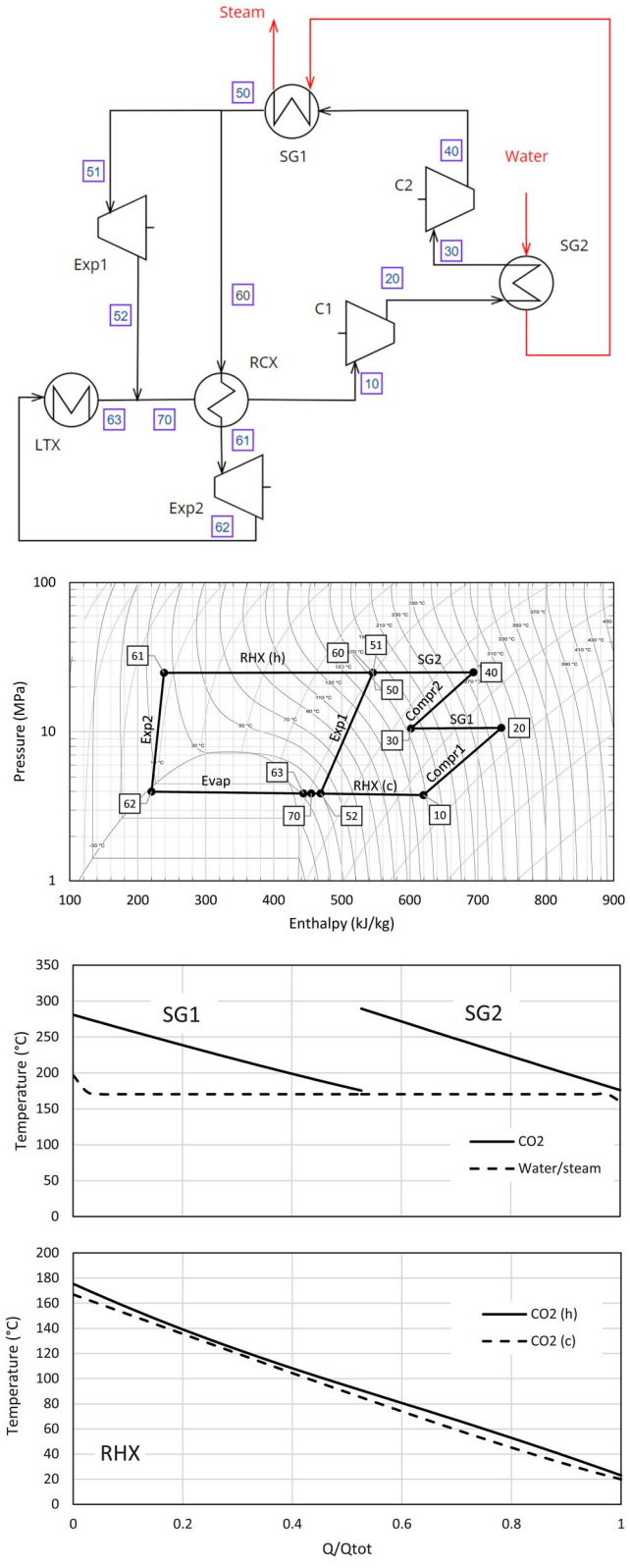

Fig. 11 CO_2 HPSG cycle process flow diagram, PH diagram, and heat exchanger TQ plots. Boxed numbers refer to state points.

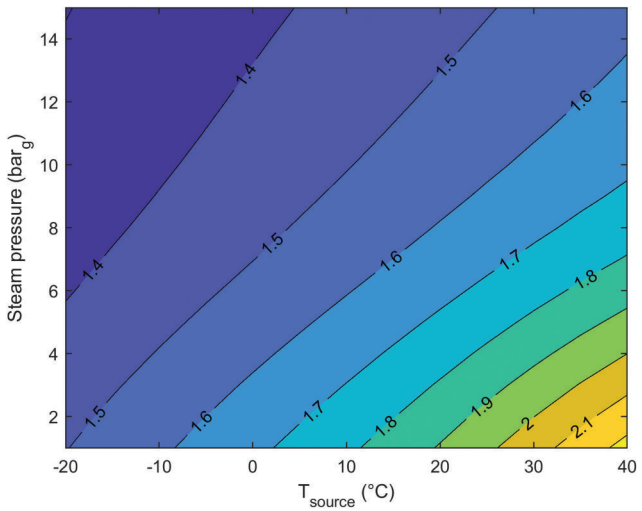

Fig. 12 Coefficient of performance map for CO_2 HPSG

- Refrigerant cost and safety: Unlike HFC and HFO refrigerants, CO_2 is not likely to be banned imminently. And unlike butane or ammonia, the flammability and toxicity risks of CO_2 are low.

3 Pilot-Scale Testing

The feasibility of both cycles has been further demonstrated experimentally at a pilot scale.

3.1 High-Temperature Heat Pump. The HTHP cycle was developed during the pilot-scale testing of an integrated pumped thermal energy storage system [18,19], that included thermal storage in a two-tank system using a commercial heat transfer fluid (HTF, Duratherm HF) (Fig. 13). A two-stage, water-cooled, oil-free reciprocating compressor (Hydro-Pac LX-series) formed the basis of the pilot-scale systems (Fig. 14), with the two stages acting in series. Due to piston seal temperature limitations, the compressor cylinders were water cooled, and a water-cooled intercooler further extracted heat between the two compressor stages. Finally, to keep the compressor inlet temperature near the ambient temperature design point, additional heat was rejected to the atmosphere in an air-cooled heat exchanger (ACC in Fig. 13).

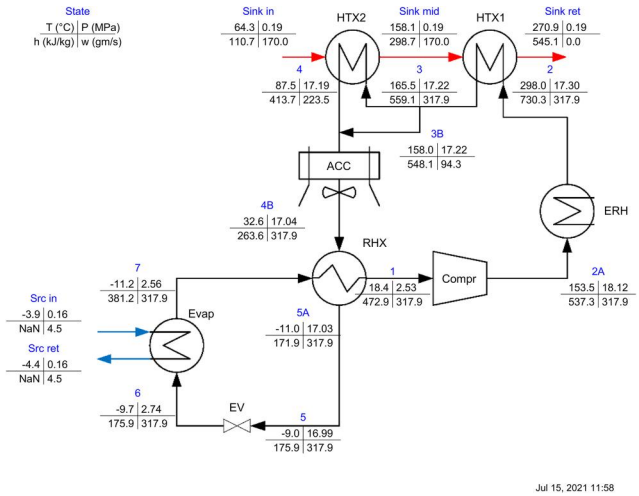

(*a*)

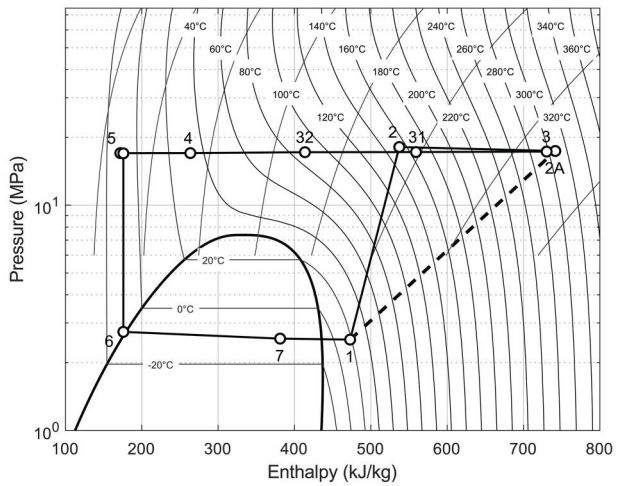

(*b*)

Fig. 13 Data from laboratory-scale CO_2 HTHP test. Dashed line in the PH diagram indicates the simulated approximate adiabatic compression path. (*a*) Process flow diagram and (*b*) pressure–enthalpy diagram.

To compensate for the nonadiabatic nature of the compressor, electric resistance heaters (ERHs) were used to simulate the temperature at the exit of an adiabatic compression process that would be typical of the larger, noncooled machines that will be used on the pilot and commercial scale HTHPs. The test configuration was designed to deliver CO_2 at a temperature of 300 °C to the heat sink. In combination with the low compressor inlet temperature requirement, the simulated adiabatic isentropic compressor efficiency was approximately 42%—well below a typical 80% isentropic efficiency that would be expected in a multi-MW scale centrifugal compressor.

At this point, the flow was then directed to a two-stage diffusion-bonded heat exchanger that transferred heat to a single-phase HTF (Duratherm HF). At an intermediate point in this heat exchanger system, a portion of the CO_2 flow was bypassed around HTX2, while the remainder transfers additional heat to the HTF. The portion of CO_2 flow diverted around HTX2 was controlled to approximately match the heat capacity ($\dot{m}c_p$) of the fluid on the two sides of the HTX, minimizing the exergy destruction and subsequent performance loss. The effect of the bypass flow on the TQ behavior in the HTX system can be clearly seen in Fig. 15, where the approximately 30% CO_2 bypass flow around the lower-temperature stage enables a significantly closer glide behavior between the two fluids.

The two flows then merged and expanded through an adiabatic valve to the low-pressure side of the system. The liquid phase CO_2 ($T_{sat} = -11\,^{\circ}C$) was then evaporated in an orbital rod evaporator [20], transferring heat from a 7% propylene glycol solution while generating an ice/water slurry. Finally, downstream of the evaporator, the CO_2 was preheated by residual heat from the high-pressure side of the system in the recuperator, a diffusion-bonded heat exchanger.

All temperatures were measured with Pt100 Class A RTDs, and pressures with Rosemount 3051 pressure transmitters. Fluid mass flowrates were measured by Micromotion Coriolis flow meters. Because the fluid at state 7 was two-phase, the enthalpy at that state was calculated based on an assumed heat balance within the recuperator.

Fig. 14 Pilot-scale HPSG using low-speed reciprocating compressor

Note that the design intent of the system was similar to the HTHP, but differed in several respects. First, to maintain the compressor inlet conditions within the manufacturer's intended limits, extra heat was rejected upstream of the high-pressure side of the recuperator in the ACC. For the same reason, the bypass flow between HTX1 and HTX2 was mixed with the HTX2 exit flow prior to the ACC and recuperator, rather than being directly used in the recuperator. As a result of these concessions, the flow exiting the evaporator and entering the recuperator was two-phase instead of a superheated vapor, an artifact of respecting compressor inlet temperature limits. In addition, due to the small scale of the system, the expander in the full-scale system is simulated with a simple control valve.

The critical outcome of the pilot-scale test was the demonstration of the interaction between the CO_2 and heat sink, in particular the use of bypass flow to glide-match the two fluids. As shown in Fig. 15, the extraction of approximately 30% of the CO_2 at the midpoint of the HTX system resulted in a close match in TQ plot slopes between the fluids.

Further testing will initially take place using the modified compressor, as described in Sec. 3.2, which allows for higher inlet and outlet temperatures. A more representative arrangement of heat exchangers will enable full validation of the HTHP architecture. Subsequently, a 500 kW_{th} pilot-scale system using ambient air as both the heat sink and heat source is in development, with commissioning expected in 2026.

3.2 Heat Pump Steam Generator. For HPSG testing, higher compressor inlet and outlet temperatures were necessary to demonstrate the cycle. The manufacturer-supplied piston seals and rider rings were replaced with a set of graphite-filled PTFE seals and rings with a usable temperature limit of approximately 200 °C. This upgrade enabled higher compressor inlet temperatures to be used, and the jacket water cooling to be eliminated, both of which resulted in a substantially higher compressor discharge temperature.

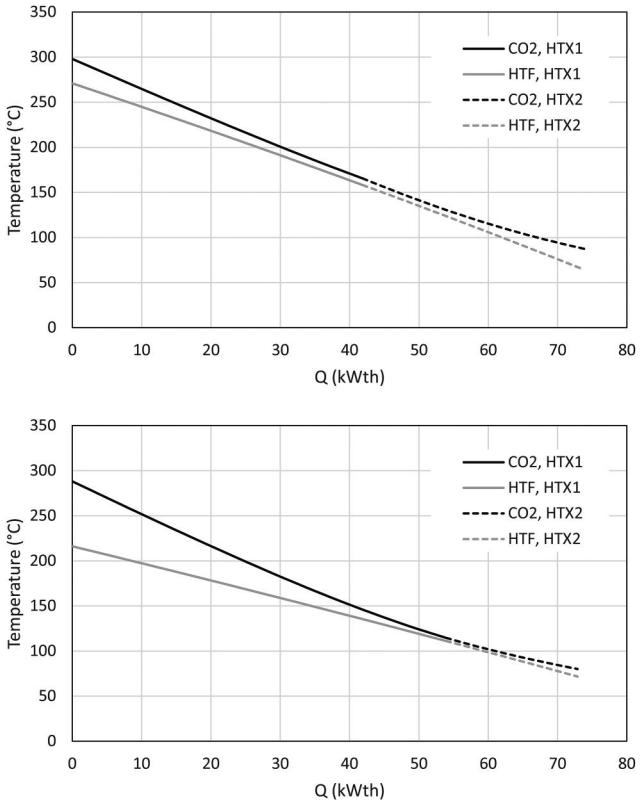

Fig. 15 Comparison of the TQ behavior in the HTX between two test conditions. In the upper figure, approximately 30% of the CO_2 flow was bypassed around HTX2, while in the lower figure, the full CO_2 flow passed through both HTX1 and HTX2.

For the steam generating heat exchangers (SG1 and SG2), a set of tube-in-tube heat exchangers (Exergy AS-00528) were used (3 in series each). Heated CO_2 flowed in the inner tube, and water/steam through the annular gap between tubes. After the first compressor stage, the heated CO_2 transferred heat to liquid water in the first set of tube-in-tube heat exchangers (SG2) then returned to the second compressor stage (C2) for further compression and heating, before returning to a second set of tube-in-tube heat exchangers (SG1) to complete the steam generation and partially cool the CO_2.

Downstream of SG1, the CO_2 flow was split into two parallel paths. Part of the flow was passed to the RCX to preheat the low-pressure CO_2 prior to entering C1. Following the recuperator, this CO_2 was expanded in a control valve to the system low-side pressure, reducing its temperature. The two-phase CO_2 was then vaporized in a brazed plate heat exchanger using 10 °C water as the heat source.

The remainder of the CO_2 was expanded directly through a parallel control valve and mixed with the vaporized CO_2 from the evaporator discharge, at which point the mixed fluid was then heated by the high-pressure CO_2 in the recuperator. By appropriate flow

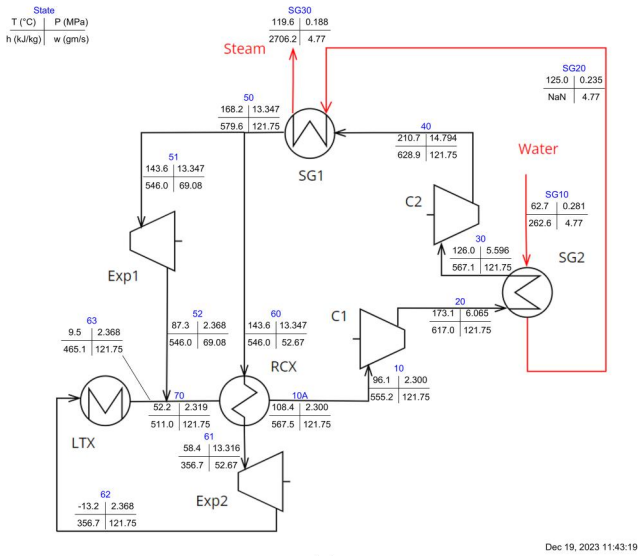

(*a*)

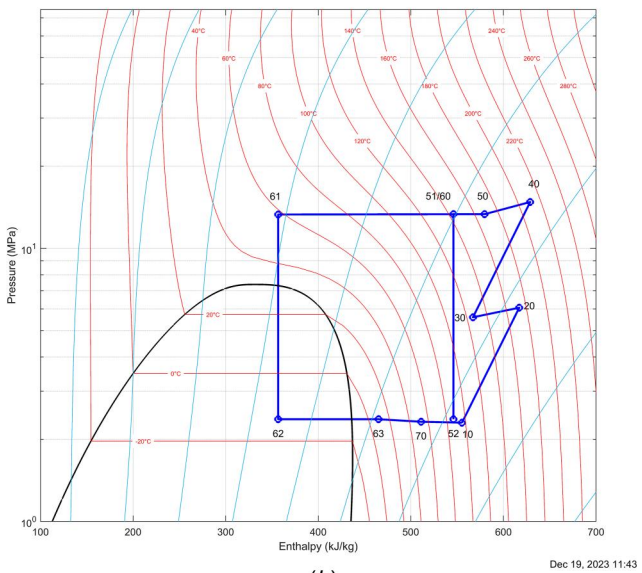

(*b*)

Fig. 16 Example pressure–enthalpy diagram of operational pilot CO_2 HPSG: (*a*) process flow diagram and (*b*) pressure–enthalpy diagram

split modulation, the heat capacity ($\dot{m}c_p$) of the fluid on the two sides of the recuperator is matched, minimizing the exergy destruction and subsequent performance loss in the recuperator.

A summary of the highest temperature operation to date is shown in Fig. 16. Active steam generation at approximately 2 barg was obtained using 10 °C water as the heat source. The upgraded compressor seals performed well over the limited duration of the test. Unfortunately, the temperature sensor at state 30 was determined to be faulty, and thus the temperature and enthalpy values at that state are estimates based on assuming that the compressor second stage (C2 in Fig. 13(*a*)) nonadiabatic efficiency is the same as for C1.

3.3 Pilot-Scale Test Summary. The purpose of the pilot-scale test system was not to achieve a particular COP, as the compressor and expanders are nonrepresentative of a full-scale system. The primary purpose of the HTHP test was to demonstrate the efficient coupling between the variable c_p of CO_2 with an essentially constant c_p fluid over a wide temperature range. This goal was achieved, as shown in Fig. 15. At the time of the HTHP test, the reciprocating compressor had significant temperature limitations that precluded its operation at the conditions a full-scale system would be able to achieve.

The successful modifications of the compressor piston seals enabled the higher-temperature testing needed to demonstrate the operating fundamentals of the HPSG cycle. Similar to the HTHP testing, the goal was not to achieve a particular COP, but rather to demonstrate the ability of the HPSG cycle to generate steam with a transcritical CO_2 cycle using a low-temperature heat source, and heat capacity matching within the recuperator as shown in Fig. 17. Further testing for both cycles is ongoing, with higher-temperature operation for the HTHP and a redesigned steam generator for the HPSG in development.

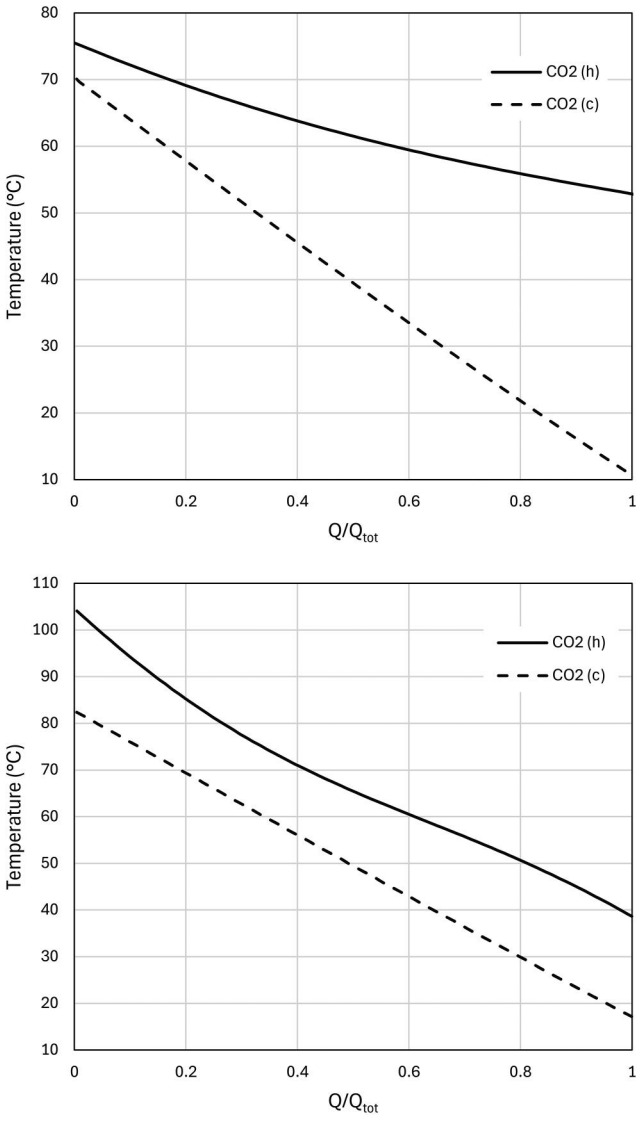

Fig. 17 TQ plots for the recuperator based on measured inlet/outlet temperatures during pilot-scale testing. The upper plot is representative of a two-stage heat pump without the high-temperature expander, while the other plot shows the TQ behavior with approximately 57% of the flow extracted through the high-temperature expander. The difference in slopes in the first figure represents a large loss in thermodynamic potential, or exergy.

4 Conclusion

Advanced high-temperature heat pumps are needed to enable the decarbonization of industrial heating. With the new CO_2 cycles described in this paper, significant gaps in industrial heat pump capability can be closed—medium-temperature (200 to 400 °C) process fluid heating, and medium pressure steam. Echogen is presently developing projects to demonstrate the HTHP cycle at pilot scale (500 kW_{th}) and the HPSG cycle at commercial scale (10 MW_{th}).

Acknowledgment

The information, data, or work presented herein was funded in part by the Advanced Research Projects Agency-Energy (ARPA-E), U.S. Department of Energy, under Award No. DE-AR0000996. The views and opinions of authors expressed herein do not necessarily state or reflect those of the United States Government or any agency thereof.

Funding Data

- U.S. Department of Energy, Advanced Research Projects Agency-Energy (ARPA-E) (Award No. DE-AR0000996; Funder ID: 10.13039/100006133).

Data Availability Statement

The datasets generated and supporting the findings of this article are obtainable from the corresponding author upon reasonable request.

Nomenclature

Roman Letters

C = heat capacity (kJ s^{-1} K^{-1})
c_p = specific heat capacity (kJ kg^{-1} K^{-1})
h = enthalpy (kJ kg^{-1})
$\dot{m}$ = mass flow rate (kg s^{-1})
Q = heat (kW)
T = temperature (K or ° C)
$\bar{T}$ = Lorenz mean temperature (K or ° C)
UA = heat exchanger conductance (K kW^{-1})

Greek Symbols

Δ = difference

Superscripts and Subscripts

c = cold
f = fluid
h = hot
LM = Lorenz mean

max = maximum
min = minimum
s = sink
sat = saturation

Acronyms

ACC = air-cooled cooler
COP = coefficient of performance
ERH = electric resistance heater
HPSG = heat pump steam generator
HTHP = high-temperature heat pump
HTX = high-temperature heat exchanger
LTX = low-temperature heat exchanger
RCX = recuperator heat exchanger
sCO_2 = supercritical carbon dioxide
SG = steam generator

References

[1] Dollinger, C., 2022, "Industrial Decarbonization Roadmap," U.S. Department of Energy, Washington, DC, Report No. DOE/EE-2635.
[2] Rissman, J., 2022, "Decarbonizing Low-Temperature Industrial Heat in the U.S.," Energy Innovation Policy and Technology LLC, San Francisco, CA, accessed Mar. 6, 2025, https://energyinnovation.org/wp-content/uploads/Decarbonizing-Low-Temperature-Industrial-Heat-In-The-U.S.-Report-2.pdf
[3] Arpagaus, C., Bless, F., Uhlmann, M., Schiffmann, J., and Bertsch, S. S., 2018, "High Temperature Heat Pumps: Market Overview, State of the Art, Research Status, Refrigerants, and Application Potentials," Energy, **152**, pp. 985–1010.
[4] Calderazzi, L., and Paliano, P. C. D., 1997, "Thermal Stability of R-134a, R-141b, R-13I1, R-7146, R-125 Associated With Stainless Steel as a Containing Material," Int. J. Refrig., **20**(6), pp. 381–389.
[5] Irriyanto, M. Z., Lim, H.-S., Choi, B.-S., Myint, A. A., and Kim, J., 2019, "Thermal Stability and Decomposition Behavior of HFO-1234ze(E) as a Working Fluid in the Supercritical Organic Rankine Cycle," J. Supercrit. Fluids, **154**, p. 104602.
[6] Trevisan, T., 2023, "European Parliament Approves Bans of HFCs and HFOs in Multiple Applications and HFC Phase Out by 2050," Brussels, Belgium, accessed Nov. 18, https://r744.com/european-parliament-approves-bans-of-hfcs-and-hfos-in-multiple-applications-and-hfc-phase-out-by-2050/
[7] Huttenlocher, D., 1992, "Chemical and Thermal Stability of Refrigerant-Lubricant Mixtures With Metals," The Air Conditioning and Refrigeration Technology Institute, Atlanta, GA, Report No. DOE/CE/23810-5.
[8] Arpagaus, C., and Bertsch, S., 2021, "Experimental Comparison of HCFO and HFO R1224 yd(Z), R1233zd(E), R1336mzz(Z), and HFC R245fa in a High Temperature Heat Pump Up to 150 °C Supply Temperature," International Refrigeration and Air Conditioning Conference, Vol. 18, Purdue University, West Lafayette, IN, May 24–28, p. 13.
[9] Siemons, R. V., 1986, "Interpretation of the Exergy Equation for Steady-Flow Processes," Energy, **11**(3), pp. 237–244.
[10] Held, T. J., 2022, "A High-Temperature, Dual Rail Heat Pump Cycle for High Performance at High Temperature Lift and Range," U.S. Utility Application 17/974,913.
[11] Held, T. J., 2015, "Supercritical CO_2 Cycles for Gas Turbine Combined Cycle Power Plants," Power Gen International, Las Vegas, NV, Dec. 8–10, p. 20.
[12] Lorenz, H., 1895, "Die Ermittelung der Grenzwerte der thermodynamischen Energieumwandlung," Z. Gesammte Kälte-Ind., **2**(8), pp. 27–32.
[13] Miller, J., Mallinak, J., and Held, T., 2021, "Supercritical Carbon Dioxide Primary Power Large-Scale Pilot Plant," Echogen Power Systems, Akron, OH, Report No. DE-FE-0031585, accessed Jan. 22, 2024, https://www.osti.gov/servlets/purl/1817332/
[14] Kaida, T., Sakuraba, I., Hashimoto, K., and Hasegawa, H., 2015, "Experimental Performance Evaluation of Heat Pump-Based Steam Supply System," IOP Conf. Ser.: Mater. Sci. Eng., **90**, p. 012076.
[15] Lemmon, E. W., Bell, I. H., Huber, M. L., and McLinden, M. O., 2018, "NIST Standard Reference Database 23: Reference Fluid Thermodynamic and Transport properties-REFPROP, Version 10.0," National Institute of Standards and Technology, Gaithersburg, MD.
[16] LDES Council, 2022, "Net-Zero Heat: Long Duration Energy Storage to Accelerate Energy System Decarbonization," Long Duration Energy Storage Council, Brussels, Belgium, accessed Dec. 15, 2022, https://www.ldescouncil.com/assets/pdf/221108_NZH_LDES%20brochure.pdf
[17] Held, T. J., 2022, "Heat Pump Steam Generator," Utility Application 18/355,541.
[18] Held, T., 2023, "Low-Cost, Long Duration Electrical Energy Storage Using a CO_2-Based Pumped Thermal Energy Storage," Echogen Power Systems, Akron, OH, Report No. DE-AR-0000996.
[19] Held, T. J., Miller, J., Mallinak, J., Avadhanula, V., and Magyar, L., 2024, "Pilot-Scale Testing of a Transcritical CO_2-Based Pumped Thermal Energy Storage (PTES) System," ASME Paper No. GT2024-129211.
[20] Gladis, S. P., Marciniak, M., O'Hanlon, J. B., and Yundt, B., 2006, "Ice Crystal Slurry TES System Using the Orbital Rod Evaporator," Liquid Ice Technology, LLC, Springfield, MO, accessed Dec. 28, 2019, https://api.semanticscholar.org/CorpusID:208173623